

# Brain Tumor Segmentation of Lower-Grade Glioma Across MRI Images Using Hybrid Convolutional Neural Networks

Amal Jlassi<sup>1</sup>, Khaoula ElBedoui<sup>1,2</sup> and Walid Barhoumi<sup>1,2</sup>

<sup>1</sup>Université de Tunis El Manar, Institut Supérieur d'Informatique, Research Team on Intelligent Systems in Imaging and Artificial Vision (SIIVA), LR16ES06 Laboratoire de Recherche en Informatique, Modélisation et Traitement de l'Information et de la Connaissance (LIMTIC), 2 Rue Abou Rayhane Bayrouni, 2080 Ariana, Tunisia

<sup>2</sup>Université de Carthage, Ecole Nationale d'Ingénieurs de Carthage, 45 Rue des Entrepreneurs, 2035 Tunis-Carthage, Tunisia

**Keywords:** Deep Learning, Brain Segmentation, MRI, LGG, Hybrid Convolutional Neural Networks.

**Abstract:** Low-Grade Gliomas (LGG) are the most common malignant brain tumors that greatly define the rate of survival of patients. LGG segmentation across Magnetic Resonance Imaging (MRI) is common and necessary for diagnosis and treatment planning. To achieve this challenging clinical need, a deep learning approach that combines Convolutional Neural Networks (CNN) based on the hybridization of U-Net and SegNet is developed in this study. In fact, an adopted SegNet model was established in order to compare it with the most used model U-Net. The segmentation uses FLuid Attenuated Inversion Recovery (FLAIR) of 110 patients of LGG for training and evaluations. The highest mean and median Dice Coefficient (DC) achieved by the hybrid model is 83% and 85.7%, respectively. The obtained results of this work lead to the potential of using deep learning in MRI images in order to provide a non-invasive tool for automated LGG segmentation for many relevant clinical applications.

## 1 INTRODUCTION

According to the World Health Organisation (WHO), Low-Grade Gliomas (LGG) are a class of grade I and grade II brain tumors. Contrary to LGG grade I, which is frequently curable by surgical resection, LGG grades II and III are infiltrative and reach to reproduce the higher-grade lesion (Louis et al., 2016). Furthermore, and as reported by WHO also, an increasing number of LGG grade II has been incidentally found through cervical MRI (Magnetic Resonance Imaging), however 3.8% to 10.4 % of patients do not have obvious tumor-related symptoms. Furthermore, in its fifth edition of 2021 relating to the classification of tumors of the central nervous system, the WHO affirms that LGG and glioneuronal tumors account more than 30% of pediatric neoplasms of the central nervous system. Thus, LGG is one of the most commonly encountered brain tumors among children, and the number of affected children may dramatically rise. Indeed, as per the data published on the site cancer.net, it is estimated that approximately 5,900 brains will be diagnosed with brain tumors this year (02/2022) in children ages 0 to 19 years in the United States. In terms of diagnosis, MRI is usually used throughout the neuro-oncology patient

treatment since routine structural imaging provides particular anatomical and pathological information. However, predicting patient outcomes based only on MRI data for these tumors are imprecise and suffers from the clinicians' inter-variability (Network, 2015). To deal with this issue, subtypes of LGG were defined across the clustering of patients based on DNA methylation, gene expression, DNA copy number, and microRNA expression (Mazurowski, 2015). Radiogenomics, as a new research direction in this field, aims to explore the relationship between tumor genomic characteristics and medical imaging such as MRI (Mazurowski, 2015). Currently, the first step when extracting tumor features was the manual segmentation of MRI by neuroradiologists or clinicians. However, manual segmentation is costly, and time-consuming, and results often lead to inter-observer variability, which can significantly sway the diagnosis. In an effort to overcome these limitations, automatic LGG segmentation seems to be one of the effective solutions. Recently, progress in Deep Learning (DL) for automatic brain segmentation has carried out a level that achieves the performance of a skilled radiologist. However, most of the existing DL works have been focused on glioblastoma, comparatively to LGG (Booth et al., 2020). Several studies

suggest that LGG can be associated with different genomic subtypes, which are significant factors in determining the course of treatment. Based on the recent literature, there is no noninvasive approach identifying genomic subtypes. Does previous literature demonstrate a correlation between LGG shape characteristics and subtypes (Buda et al., 2019). In fact, it leads to conducting radiogenic analysis and enhances inferences about these correlations.

In this work, we propose a fully automated segmentation method that identify whether the assessed shape features are prognostic of tumor molecular subtypes or not. To do so, the proposed method is based on an integrated deep learning architecture combining SegNet and U-Net architectures. In fact, to the best of our knowledge, none of the state-of-the-art methods have tested the performance of the well-known CNN architecture SegNet on delineating LGGs. Most of the literature methods are based on U-Net variants which have shown promising performances. Thus, in order to take advantage of the benefits of both U-Net and SegNet algorithms, we have conducted a comparative study which allowed us to propose an effective method that combines both architectures in order to further enhance the diagnosis accuracy. Literally, this work aims to investigate the correlation between selected shape features and genomic subtypes in order to provide the information to clinicians sooner via a non-invasive method. Further, in some cases, it could perform better delineation of tumors where the resection is not provided. Indeed, the obtained results show that the proposed automated tool based on deep learning could be helpful for the diagnosis and the treatment planning of LGG.

The remainder of this paper is organized as follows. Section 2. describes the state of the art whereas section 3. presents the proposed hybrid CNN architectures for segmenting LGG from MRI images. Then, in section 4. we show results for the segmentation model. In section 5. we produce a conclusion with some directions.

## 2 RELATED WORK

Various segmentation approaches have been developed to delineate LGG on MRI scans. The vast majority of these approaches are based on machine learning. For instance, generative and discriminative models have been widely used. On the one hand, Generative Models (GMs) have the capacity to handle small-

sized datasets. On the other hand, Discriminant Models (DMs) are more efficient when using "wide data". However, GMs are generally less accurate than DMs.

### 2.1 Generative Models

GMs such as atlas-based models need prior knowledge of anatomy and take on posterior probabilities for voxels' classification. For instance, Parisot et al. have explored firstly prior knowledge in order to classify the tumor then they used another graph to identify the class of each voxel (Parisot et al., 2012). However, Huang et al. have used the sparseness of samples to construct a particular dictionary and develop a softmax model in order to optimize the error reconstruction coefficients for different classes (Huang et al., 2014). Furthermore, the Random Forest (RF) approach, notably in the cases of high number of features, has succeeded to be good to accomplish accurate brain tumor segmentation (Zikic et al., 2012). In this context, Meier et al. have used a set of dedicated features-based decision RF to discriminate pathological regions within brain MRI volumes (Meier et al., 2015). Likewise, Meier et al. have investigated the CRF method to improve the voxel-wise classification accuracy on the summit of the RF classifier. Differently, Markov Random Field (MRF) and Conditional Random Field (CRF) are also frequently used for brain tumor segmentation. For instance, Zhao et al. have proposed a semi-segmentation approach based on the MRF, in which one slice was labeled and the other slices were sequentially labeled using the MRF label (Zhao et al., 2013). Nevertheless, GMs usually focus on the distribution of a dataset in order to return a probability for a given example.

### 2.2 Discriminative Models

DMs, such as the Support Vector Machine (SVM), do not require prior knowledge of anatomy and use imaging features extracted from MRI instead of the original MRI data for the classification task. Thus, dimensionality reduction or imaging feature selection is mostly developed before the model training task. Deep Learning (DL) based on CNN is a promising approach that is different from classical DMs since it is based on end-to-end classifiers. In fact, unlike classical DM, imaging feature extraction and selection is automated during model training, and this approach has shown relevant results in automatic tumor segmentation. Furthermore, in recent years, CNN models have shown promising performances in medical image processing, not only in terms of accuracy but also in terms of efficiency. Pereira

et al. have developed two different structures with dissimilar depths to deal with the LGG (Thaha et al., 2019). Similarly, Dvorak et al. have evaluated the effectiveness of different patch selection techniques based on the segmentation results of CNNs (Zhang et al., 2020). Havaei et al. have proposed a multiscale CNN structure in order to enhance the use of local and global information (Havaei et al., 2015a). A combination of RF with the final output of CNNs is used to make better classification results. Zhao et al. have introduced a method that combines FCNN and CRF (Havaei et al., 2015b). The main advantage of this method is that it treats the subproblem of unbalanced data. Overall, the patches are often randomly extracted with controlling their number per class. However, the size or quality of the patches can affect easily the LGG segmentation. For example, a patch of a small size cannot have all the spatial information whereas a patch of considerable size will need more computational resources. To address these problems, recent studies used CNN-based encoder-decoder networks. For instance, Buda et al. have recently proposed a fully automatic way to quantify LGG characteristics using U-Net architecture and test whether these characteristics are predictive of tumor genomic subtypes (Buda et al., 2019). Due to the excellent performance of U-Net, other segmentation networks based on the U structure of U-Net are produced such as UNet++. Xu et al. have proposed an LGG segmentation tool based on the UNet++ model (Xu et al., 2020) which uses nested dense skip connections to reduce the semantic gap between encoder and decoder caused by the U-Net model. Moreover, Naser et al. have combined CNN based on the U-Net for LGG segmentation and transfer learning based on a pre-trained convolution-base of Vgg16 and a fully connected classifier (Naser and Deen, 2020). The latter U-Net architecture uses skip connections to the corresponding layers in the decoding part. Thus, it leads to a shortcut for gradient flow in shallow layers during the training task. More recently, two models, which are U-Net with a ResNeXt-50, have been investigated in (Paradkar and Paradkar, 2022). This work includes analyzing LGGs through deep learning-based segmentation, shape feature extraction, and statistical analysis to identify correlations between selected shape features and genomic subtypes.

As best as we know, no CNN architecture based on SegNet is used for LGG segmentation. The most used one is the U-Net model which requires higher computational time compared to SegNet. However, the skip connection saddles the set of captured fea-

tures to the corresponding upsampling convolution blocks in the SegNet decoder module. This paper focuses on the hybridization of the CNN architecture, the hybrid U-SegNet. The idea comes after a comparative study between U-Net and SegNet models. Thus, the proposed architecture is a U-shape model with properties mimicked from the SegNet.

### 3 MATERIALS AND METHODS

In this section, we firstly present the dataset that we investigated in this work. Then, the proposed method for the LGG segmentation is described comparatively to used SegNet and U-Net and evaluated within the used dataset.

#### 3.1 Materials

The dataset used in this study contains brain MR images together with manual FLAIR abnormality segmentation masks. The images were obtained from The Cancer Imaging Archive (TCIA). In fact, these scans correspond to 110 patients included in The Cancer Genome Atlas (TCGA) LGG collection with fully FLAIR sequence and genomic cluster data available. The collection of patients comes from five different institutions (Thomas Jefferson University – 16 patients; Henry Ford Hospital – 45 patients; UNC – 1 patient; Case Western – 14 patients; and Case Western St. Joseph’s – 34 patients). The patients are distributed as 50 patients with Grade II, and 58 patients with Grade III. Figure 1 summarises the characteristics of the patient’s data such as tumor grades, tumor sub-types, genders, and ages. Each MRI per patient contains from 20 to 88 slices with the size of 256 pixels and shows cross-sectional areas of the brain as shown in Figure 2. Tumor shape assessment was based only on the FLAIR abnormality since tumor enhancement in LGG is infrequent. The Ground Truth (GT) generated by tumor masks was performed by Buda et al. (Buda et al., 2019) using the FLAIR MRI images and they made it publicly available for download from (<https://www.kaggle.com/>).

#### 3.2 Methods

An overview of the proposed approach used for LGG segmentation is shown in Figure 3. In fact, the proposed fully automatic method of LGG segmentation based on a hybrid CNN is composed of three main procedures: image preprocessing, data augmentation, and segmentation.

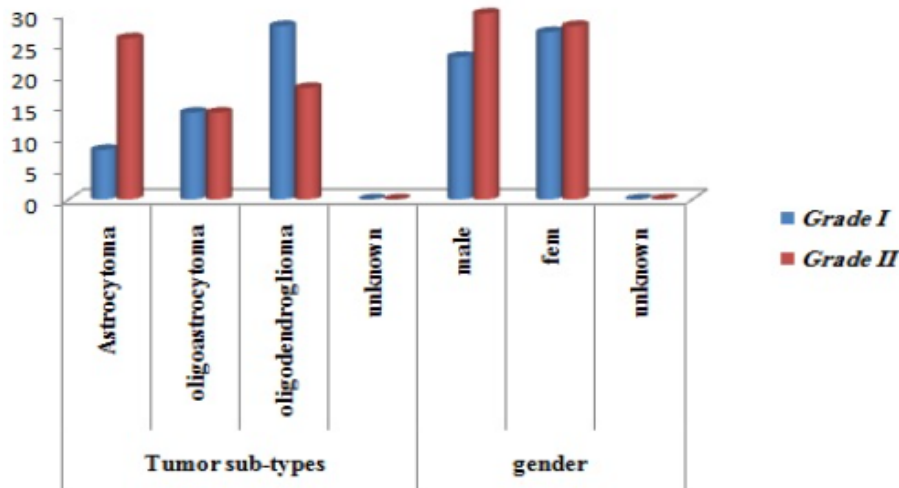


Figure 1: The patients' data includes tumor grades, tumor sub-types, genders, and ages.

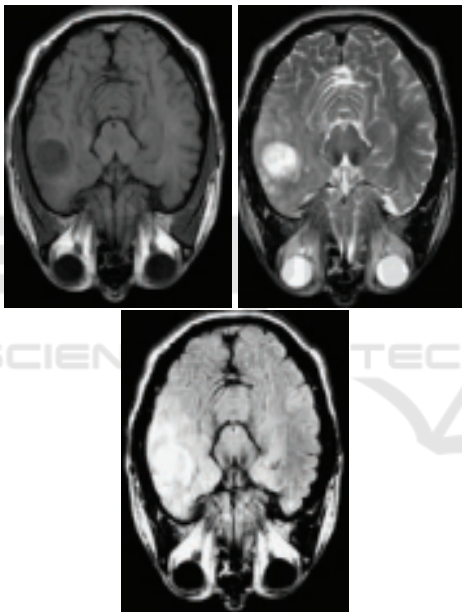


Figure 2: A sample of MRI scans from the TCGA dataset: (a) T1 modality, (b) T2 modality, and (c) FLAIR modality).

### 3.2.1 Preprocessing

The Skull Stripping (SS) process is used in order to extract brain tissue from the non-brain tissue. The output of the SS is a new image with only a brain pixel (without non-brain tissue) as presented in Figure 4 or a binary value assigning value 1 for brain pixels and value 0 for the rest of the tissue. More precisely, the preprocessing of the MRI sequences consists of the following steps:

1. Scaling images to the joint frame of reference.
2. Stripping of the skull to concentrate the analysis

of the brain region.

3. Normalizing the tissue intensity.

### 3.2.2 Data Augmentation

The number of images containing tumors was significantly lower than the number of those with only background class present. To deal with this issue, data augmentation seems to be a good solution. However, in our context, we cannot apply all transformations because the segmentation results could considerably change. Consequently, we opted to work on three possible transformations in order to not degrade the training performance (Buda et al., 2018). Indeed, for each oversampled slice, we applied random rotation, flip and for the other slice, we applied random scale, as shown in Figure 5. Finally, in order to reduce the unbalance between tumor and non-tumor classes, we isolated empty slices that did not contain any brain or other tissue after applying the Skull Stripping process.

### 3.2.3 Segmentation

Recently, deep neural networks are payoff popularity among researchers and have shown outstanding performance with appreciated accuracy in medical image segmentation. CNN is a type of deep neural network, which can learn and extract features from images. In fact, many researchers have used CNN for automatic brain tumor segmentation in MRI images, especially for LGG segmentation. The objective of this paper is to generally explore the CNN architectures for brain tumor segmentation and specifically those of SegNets and U-Net. So, it is important to find the relevant advantages of each model in order

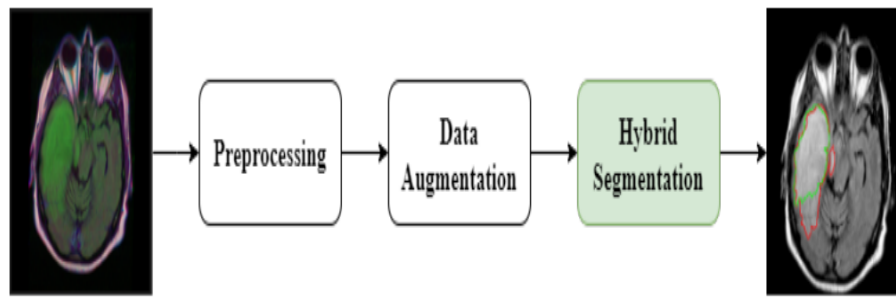


Figure 3: An overview of the proposed hybrid CNN.

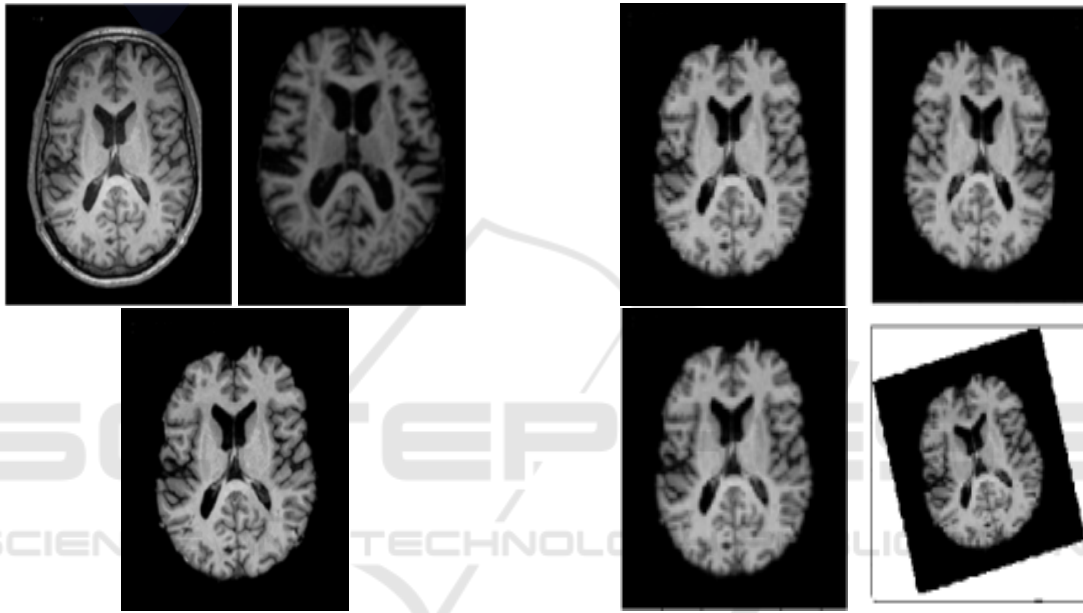


Figure 4: Preprocessing Example: (a) Original MRI, (b) Skull Stripped MRI, and (c) Preprocessed MRI.

Figure 5: Example of corresponding data augmentation results. (a) Original MRI. (b) Flip. (c) Scale by 4%–8%. (d) rotation by 5°–15°.

to develop a hybrid architecture by inheriting the advantages of these models. It is noticeably expected that the hybrid architecture will give a more devoted result. Particularly, U-Net has achieved good results in medical image segmentation. Hence, it is the most commonly used in the LGG segmentation task. It has performed outstanding results in this challenge and it has overcome the problems of fewer data capacity, fuzzy boundaries, and high gray scales in medical image analysis. In fact, the U-Net method includes an encoder for processing input MRI images and a decoder for generating outputs (Drozdzal et al., 2016). Firstly, the encoder decomposes the image into different levels of feature maps. Then, it extracts the coarse-grained features of the main feature maps. Next, the decoder restores the feature maps of each layer by an up-sampling process. The concatenation cascades the features of each layer of the encoder with

the features obtained by the transpose convolution operation in the decoder. Thus, it reduces the loss of accuracy in the feature extraction process. Regarding the SegNet, it can be classified based on the number of convolution blocks (Li et al., 2021). The SegNet basically, has two convolutional layers with  $3 \times 3$  filters. In each convolution block, the feature extraction and the convolution operation are performed from the input by sliding the filter kernel. Moreover, batch normalization layers are developed after each convolutional layer in order to normalize the channels of the extracted features. Moreover, ReLU layers are used in order to convert the negative value to zero without changing its dimensions. It seems that U-Net is able to capture fine and soar pieces of information from the encoder to the decoder using skip linking, but it requires a higher computational time compared to SegNet. Since none of the state-of-the-art works

have tested the performance of the well-known CNN architecture SegNet on delineating LGGs. A comparative study is established between the U-Net used by Buda et.al (Buda et al., 2019) and the SegNet. The latter is composed of an encoder network and a corresponding decoder network, followed by a final classification layer in pixels. This architecture is illustrated in Figure 6. In our case, the encoder network consists of 10 layers followed by encoders, of the same number of blocks set-top boxes.

In order to keep the higher-resolution feature maps at the deepest encoder output, fully connected layers were removed. The final decoder output is fed to a Sigmoid classifier to produce class probabilities for each pixel independently. For our dataset, the SegNet architecture is trained with various parameters and then we chose the relevant ones that gave a promising result for our task. The developed SegNet has the following encoder layers:

- Input: MRI scans.
- Conv-1: The convolutional layer consists of 16  $3 \times 3$  filters applied with a stride of 1 and a padding of 1.
- Conv-2: The convolutional layer consists of 16 filters of size  $3 \times 3$  applied with a stride of 1 and padding of 1.
- MaxPool-1: The next maxpool layer of Conv-2 consists of a size pool of  $2 \times 2$  and a stride of 2.
- Conv-3: The convolutional layer consists of 32 filters of size  $3 \times 3$  applied with a stride of 1 and padding of 1.
- Conv-4: The convolutional layer consists of 32 filters of size  $3 \times 3$  applied with a stride of 1 and padding of 1.
- MaxPool-2: The next maxpool layer Conv-4 consists of a size pool of  $2 \times 2$  and a stride of 2.
- Conv-5: The convolutional layer consists of 64 filters of size  $3 \times 3$  applied with a stride of 1 and a padding of 1.
- Conv-6: The convolutional layer consists of 64 filters of size  $3 \times 3$  applied with a stride of 1 and a padding of 1.
- MaxPool-3: The next maxpool layer of Conv-6 consists of a size pool of  $2 \times 2$  and a stride of 2.
- Conv-7: The convolutional layer consists of 128 filters of size  $3 \times 3$  applied with a stride of 1 and a padding of 1.
- Conv-8: The convolutional layer consists of 128 filters of size  $3 \times 3$  applied with a stride of 1 and padding of 1.
- MaxPool-4: The next maxpool layer of Conv-8 consists of a size pool of  $2 \times 2$  and a stride of 2.
- Conv-9: The convolutional layer consists of 256 filters of size  $3 \times 3$  applied with a stride of 1 and a padding of 1.
- Conv-10: The convolutional layer consists of 256 filters of size  $3 \times 3$  applied with a stride of 1 and a padding of 1.
- MaxPool-5: The next max pool layer of Conv-10 consists of a size pool of  $2 \times 2$  and a stride of 2.

Furthermore, the hyperparameters adopted for the training process of this model are as follows: learning Rate (LR) equals to 0.0001, number of epochs equals to 100, lot size equals to 16, and Adam as optimization algorithm.

As mentioned above, the objective of this work is to combine the popular deep CNN models which are U-Net and SegNet for the automatic segmentation of tumors in the brain MRI images, by exploring the advantages of each model. The proposed U-SegNet is a hybridization of U-Net architecture which is widely used for LGG segmentation and SegNet architecture. Figure 7 shows the U-SegNet architecture which is an assembly model that combines the U-Net and SegNet architectures.

Similarly to U-Net, the U-SegNet architecture is a U-shaped model with image features trained at different levels through a set of convolution and pooling layers. The decoder layer uses the pooling indices from the max-pooling step corresponding to the encoder layer's role to oversample the low-level feature maps instead of the deconvolution layers. We used the same parameters of SegNet to implement U-SegNet. Additionally, we used 10 encoder blocks and 10 decoder blocks. Batch normalization and ReLu activation functions were applied on the feature maps after the filters were applied in the encoder branch. A U-Net type hop connection is only provided at the upper layer, as shown in Figure 7, in order to insert feature maps with fine detail. The jump connection helps us to introduce fine information without increasing the parameters as it was done in U-Net. Finally, a Sigmoid layer is used in order to produce class probabilities for each pixel independently. The hyperparameters adopted for the training process of this model are as follows: learning rate equals to 0.0001, number of epochs equals to 100, a lot size of 16, Stall (Momentum) equals to 0.5, and Adam as an optimization

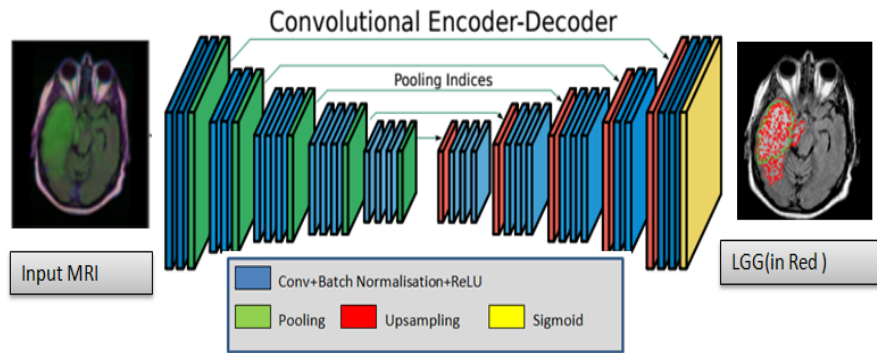


Figure 6: An illustration of the SegNet architecture generated while highlighting the LGG region (in Red). There are no Fully Connected (FC) layers and only convolutional layers are used.

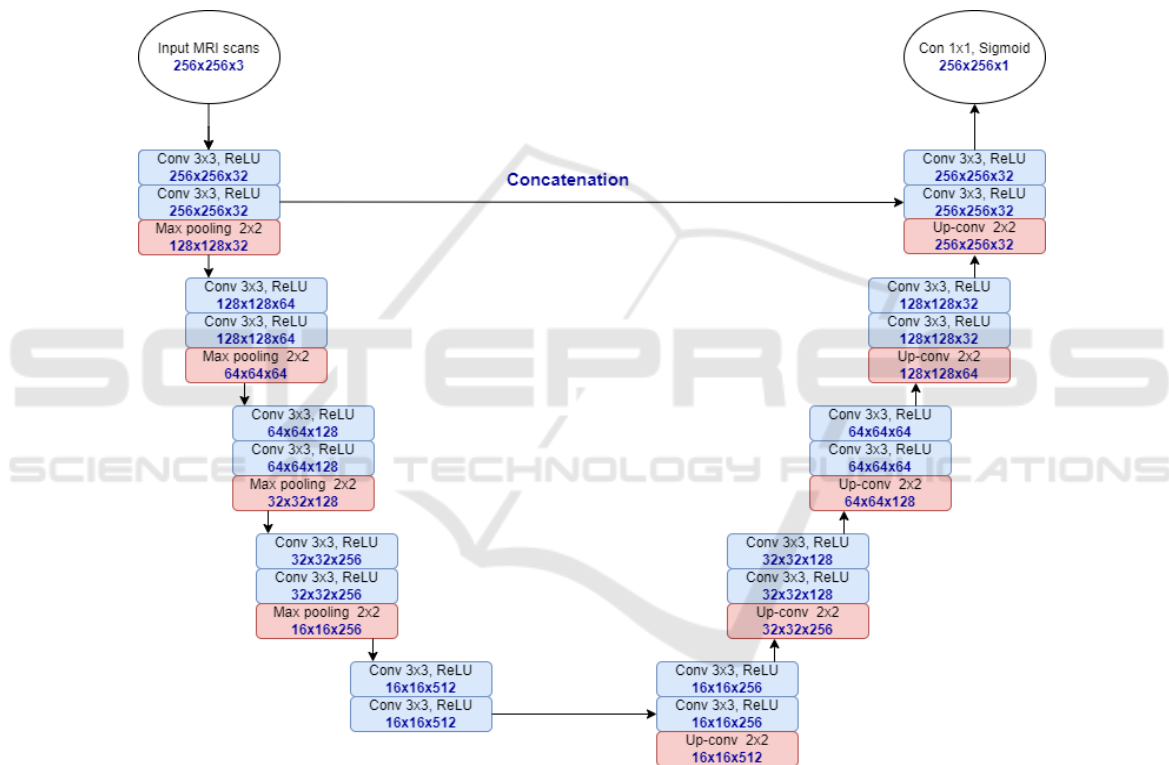


Figure 7: U-SegNet architecture used for segmentation. Below each layer specification dimensionality of a single example that this layer outputs were provided.

algorithm.

The segmentation model used in this work was based on CNN with the hybrid architecture. In order to improve the learning performance, we have implemented the U-SegNet architecture. This architecture is a new model based on the SegNet model with a connection hop to the upper layer to retrieve the finer details of the feature map. Moreover, we have introduced dropout in the encoder layer which is a regulation technique in order to avoid overfitting (increase validation accuracy). We have chosen what gives the

model a better opportunity to learn independent representations. Typically, using a small dropout value of 20-50% of neurons is sufficient, with 20% being a good starting point. Too low a value has minimal effect and too high a value leads to under-training of the network. As shown in Figure 7, the U-SegNet consists of 5 blocks of layers which contain 2 convolution layers (in blue color) with ReLU activation function and one max pooling layer (in pink color) in the encoding (down-sampling) part and a similar 5 blocks of layers but with one convolution transpose

layer (in pink color) instead of max pooling in the decoding (up-sampling) part. The number of filter channels and the image size are given at the bottom of each layer. The size of the input layer (in white color) is  $256 \times 256 \times 3$  and the size of the output layer is  $256 \times 256 \times 1$  which is a convolution layer with Sigmoid activation function.

## 4 EXPERIMENTAL RESULTS

In order to evaluate the performance of the proposed method, various experiments have been performed on a challenging MRI dataset. We have used the following libraries for the implementation: OpenCV, Pillow, NumPy, Matplotlib, and TensorBoard for visualization. The operating system used was Ubuntu 18.04 on a computer with 5 cores and with an Nvidia GeForce GTX 960M graphics processor equipped of 9 GB of RAM. This section includes qualitative and quantitative assessment of the proposed method, while comprehensively assesses each module of the method.

### 4.1 Qualitative Evaluation

To illustrate the performance of the segmentation model, overlays of FLAIR MRI images with the outlines of tumor masks using manual and model segmentations for the test datasets are shown in Figure 8. Each panel, in Figure 8, is showing the highlighted tumor in red, while the overlay image with tumor outlines (green – manual segmentation and red – model segmentation). Overall, the visualization of the results allowed us to see that U-Net and SegNet make complementary errors. Representative examples of automatic segmentation results obtained using SegNet architecture with best and worst scores are shown in Figure 9 and Figure 10, respectively. The results reflect the anomalous detection of regions, while noise and random speckles (red dots) indicate that SegNet tends to miss finer details. It is clear that the proposed model lacks precision, although it considers very deep with 10 encoder layers. However, the proposed model has succeeded in detecting the glioma region even in the worst case, but it lacks precision. This leads us to think that it lacks regularization to fit the proposed problem. This will be discussed in the next part. In fact, while visualizing the results, we have observed that the proposed U-SegNet architecture captures fine details and solves the random noise problem seen in SegNet as illustrated in Figure 11 and Figure 12. It is obvious that adding skip connections to the upper layers helps to improve performance.

Consequently, SegNet tends to miss the finer de-

tails and in some cases suffers from random noise. On the other hand, U-Net, thanks to jump connections, is able to capture fine details; i.e. borders; more accurately than SegNet. However, as shown in the same figure (Figure 8), U-Net makes some errors in the detection of tumors. We suspect this is due to confusion created by deconvolutional layers and skipped connections at lower levels. Moreover, compared to U-Net, U-SegNet has fewer parameters than U-Net allowing our network to train better. This solves the accuracy problem. Although SegNet tends not to have access to finer details, the proposed model is able to capture these finer details by integrating the single hop connection into the U-SegNet architecture.

### 4.2 Quantitative Evaluation

To compare the quantitative performances of the different models, we have evaluated the performance of these segmentations through the Dice similarity (DC) coefficient. It is among the most widely used metrics for brain tumor and structure segmentation applications. The Dice coefficient (1) was used to evaluate the similarity of the predicted tumor masks by the segmentation model with the tumor masks obtained by manual segmentation (GT).

$$DC = \frac{2 \times TP}{2 \times TP + FN + FP}, \quad (1)$$

where, TP, FP, and FN represent respectively the True Positive, False Positive, and False Negative of the class for which the result is calculated.

Table 1 shows the training time, best Dice coefficient, mean Dice coefficient, and median Dice coefficient of each model per 100 epochs. As shown in Table 1, SegNet performs faster than other models since SegNet uses only max-pooling indices to oversample low-level features. It is obvious that adding skip connections to the upper layers helps to improve the performance. Thus, U-SegNet gave an average Dice value of 83% and a median Dice coefficient of 86%. Network training required 8 GB of memory while the total training time was approximately 5 hours and 58 minutes. In Figure 13, we present the loss and Dice convergence results of the validation dataset for each of these models. Both U-Net and U-SegNet models seem to be doing quite well. However, according to the same Figure 13, the predictions vary for complex images with extremely diversified sub-regions. In addition, it is clear that U-SegNet is good at predicting regions in images that are very difficult and complex. Interestingly, U-SegNet incorporates the good features of both U-Net and SegNet architectures. Compared to U-Net, U-SegNet has fewer

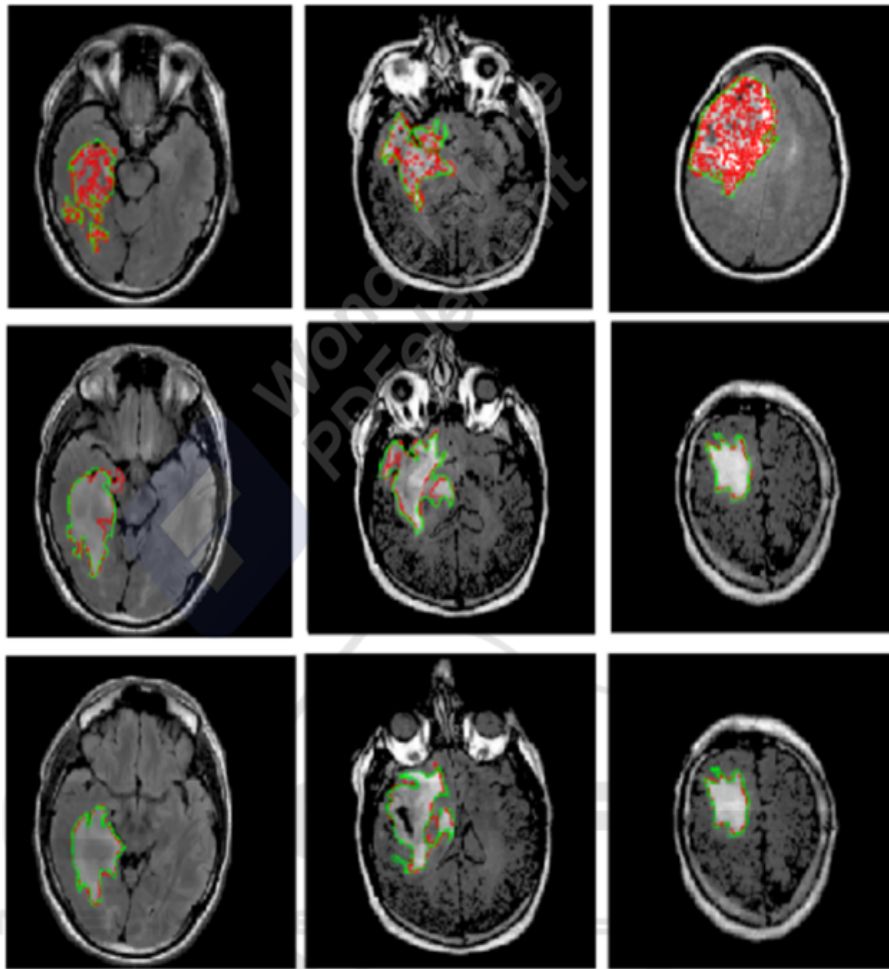


Figure 8: Samples from the test data sets showing FLAIR images for highlighted LGG regions and overlays of FLAIR images and tumor masks' (GT) (green – manual segmentation and red – model segmentation). First line: segmented LGG using U-Net architecture. Second line: segmented LGG using SegNet. Third line: segmented LGG using proposed U-SegNet.

Table 1: Evaluation of the proposed architecture comparatively to the U-Net and the SegNet architectures (best values are in bold).

Models	Time	Best DC	Mean DC	Median DC
U-Net [(Buda et al., 2019)]	8 :02 :35	90 %	82%	85 %
SegNet	<b>4 :40 :50</b>	84 %	76 %	78 %
U-SegNet	5 :57 :42	<b>91,3 %</b>	<b>83%</b>	<b>85,7 %</b>

parameters than U-Net which allows it to be trained better. This solves the accuracy problem. Although SegNet does not tend to have access to finer details, the proposed model is able to capture these finer details by integrating the single hop connection into the U-SegNet architecture.

## 5 CONCLUSION

In this work, we have investigated three relevant models, namely U-Net, SegNet, and U-SegNet designed for reliable automatic LGG segmentation from MRI images. The proposed hybrid model inherits the properties of U-Net and SegNet, which are the most popular CNN models for medical image segmentation. In the case of LGG tumors, small sizes are lost during subsampling, resulting in inappropriate segmenta-

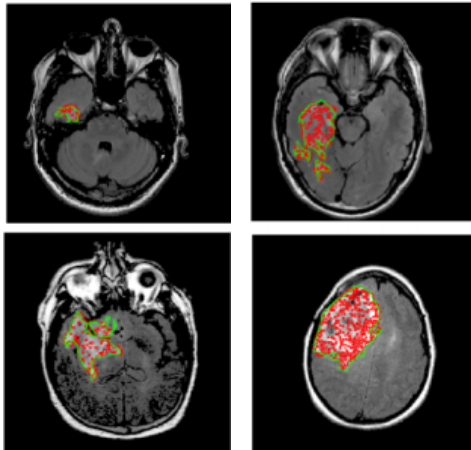


Figure 9: Example of segmentation results by SegNet with Ground Truth (in Green) for the best cases.

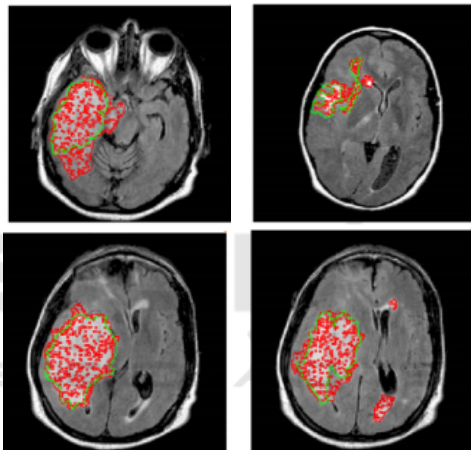


Figure 10: Example of segmentation results by SegNet overlays of FLAIR images and tumor masks' (GT) (green – manual segmentation and red – model segmentation) for the worst cases.

tion. The hybrid model can overcome such a problem by adding a hop connection to the upper layer of the SegNet, in order to retrieve the finer details from the feature map. All CNN models (U-net, SegNet, and U-SegNet) have been trained and validated using the challenging TCGA dataset. The performance of the proposed hybrid model in terms of average Dice coefficient was 83%, a value that exceeds that of each model apart. This was achieved through deep learning architecture that coupled the advantages of U-Net with those of the SegNet. This study may be the first step in order to associate the imaging features of LGG and molecular tumor subtypes established by genomic analysis. The proposed model shows promise as a non-invasive tool for tumor characterization in LGG. Furthermore, there are several

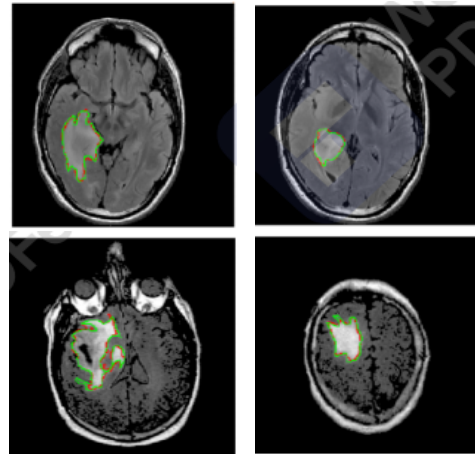


Figure 11: Example of segmentation results by U-SegNet overlays of FLAIR images and tumor masks' (GT) (green – manual segmentation and red – model segmentation) for the best cases.

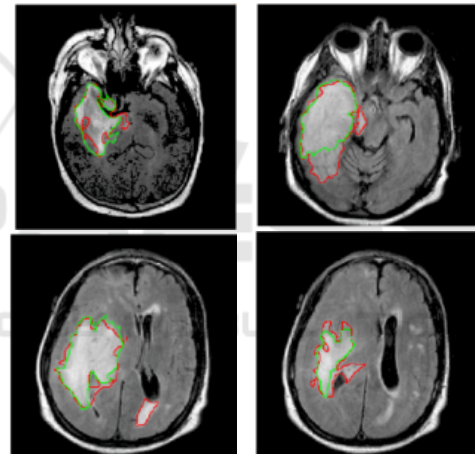


Figure 12: Example of segmentation results by U-SegNet overlays of FLAIR images and tumor masks' (GT) (green – manual segmentation and red – model segmentation) for the worst cases.

techniques for developing automatic segmentation of brain tumors that could be inspected for comparison and to further enhance the obtained results (Akkus et al., 2017). The LGG data used for validation is comparatively small and there were not more datasets available for testing. However, in order to generalize proposed models, additional datasets should be used for more accurate evaluation. Nevertheless as a next step, we will analyze the relationship between the imaging features and genomic clusters.

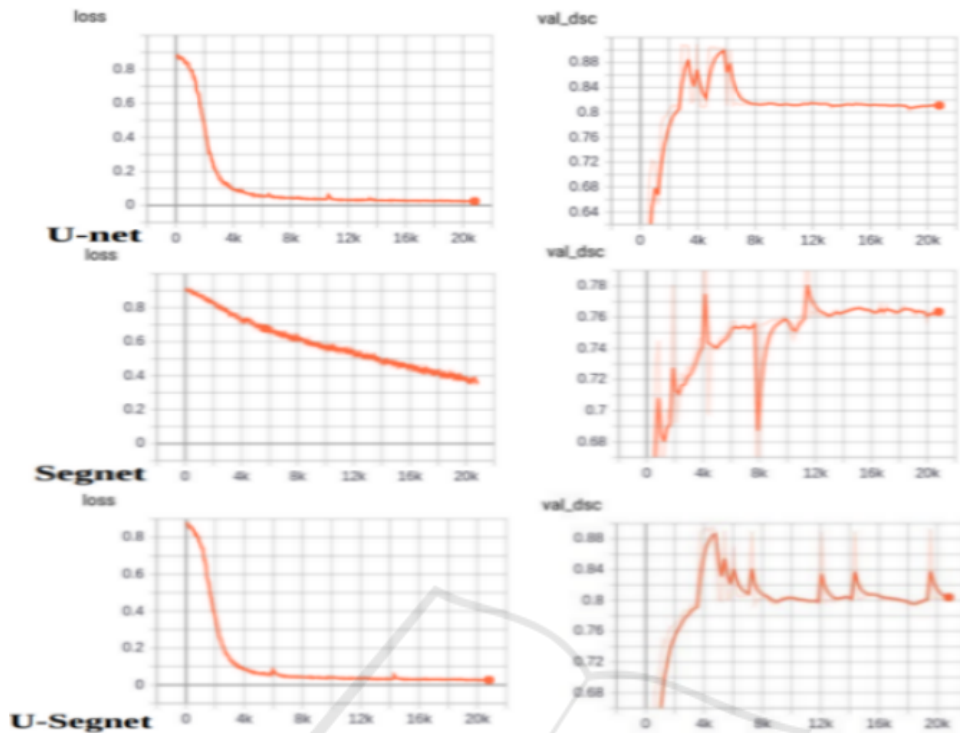


Figure 13: Evaluation of loss and DSC convergence of selected automatic LGG segmentation methods: U-Net, SegNet, and U-SegNet.

## REFERENCES

- Akkus, Z., Galimzianova, A., Hoogi, A., Rubin, D. L., and Erickson, B. J. (2017). Deep learning for brain mri segmentation: state of the art and future directions. *Journal of digital imaging*, 30(4):449–459.
- Booth, T. C., Williams, M., Luis, A., Cardoso, J., Ashkan, K., and Shuaib, H. (2020). Machine learning and glioma imaging biomarkers. *Clinical radiology*, 75(1):20–32.
- Buda, M., Maki, A., and Mazurowski, M. A. (2018). A systematic study of the class imbalance problem in convolutional neural networks. *Neural networks*, 106:249–259.
- Buda, M., Saha, A., and Mazurowski, M. A. (2019). Association of genomic subtypes of lower-grade gliomas with shape features automatically extracted by a deep learning algorithm. *Computers in biology and medicine*, 109:218–225.
- Drozdal, M., Vorontsov, E., Chartrand, G., Kadoury, S., and Pal, C. (2016). The importance of skip connections in biomedical image segmentation. In *Deep learning and data labeling for medical applications*, pages 179–187. Springer.
- Havaei, M., Dutil, F., Pal, C., Larochelle, H., and Jodoin, P.-M. (2015a). A convolutional neural network approach to brain tumor segmentation. In *BrainLes 2015*, pages 195–208. Springer.
- Havaei, M., Dutil, F., Pal, C., Larochelle, H., and Jodoin, P.-M. (2015b). A convolutional neural network approach to brain tumor segmentation. In *BrainLes 2015*, pages 195–208. Springer.
- Huang, M., Yang, W., Wu, Y., Jiang, J., Chen, W., and Feng, Q. (2014). Brain tumor segmentation based on local independent projection-based classification. *IEEE transactions on biomedical engineering*, 61(10):2633–2645.
- Li, G., Liu, Q., Ren, W., Qiao, W., Ma, B., and Wan, J. (2021). Automatic recognition and analysis system of asphalt pavement cracks using interleaved low-rank group convolution hybrid deep network and segnet fusing dense condition random field. *Measurement*, 170:108693.
- Louis, D. N., Perry, A., Reifenberger, G., Von Deimling, A., Figarella-Branger, D., Cavenee, W. K., Ohgaki, H., Wiestler, O. D., Kleihues, P., and Ellison, D. W. (2016). The 2016 world health organization classification of tumors of the central nervous system: a summary. *Acta neuropathologica*, 131(6):803–820.
- Mazurowski, M. A. (2015). Radiogenomics: what it is and why it is important. *Journal of the American College of Radiology*, 12(8):862–866.
- Meier, R., Karamitsou, V., Habegger, S., Wiest, R., and Reyes, M. (2015). Parameter learning for crf-based tissue segmentation of brain tumors. In *BrainLes 2015*, pages 156–167. Springer.

- Naser, M. A. and Deen, M. J. (2020). Brain tumor segmentation and grading of lower-grade glioma using deep learning in mri images. *Computers in biology and medicine*, 121:103758.
- Network, C. G. A. R. (2015). Comprehensive, integrative genomic analysis of diffuse lower-grade gliomas. *New England Journal of Medicine*, 372(26):2481–2498.
- Paradkar, R. and Paradkar, R. (2022). Analysis of lower-grade gliomas in mri through segmentation and genomic cluster-shape feature correlation. *bioRxiv*.
- Parisot, S., Duffau, H., Chemouny, S., and Paragios, N. (2012). Graph-based detection, segmentation & characterization of brain tumors. In *2012 IEEE Conference on Computer Vision and Pattern Recognition*, pages 988–995. IEEE.
- Thaha, M. M., Kumar, K., Murugan, B., Dhanasekeran, S., Vijayakarthish, P., and Selvi, A. S. (2019). Brain tumor segmentation using convolutional neural networks in mri images. *Journal of medical systems*, 43(9):1–10.
- Xu, D., Zhou, X., Niu, X., and Wang, J. (2020). Automatic segmentation of low-grade glioma in mri image based on unet++ model. In *Journal of Physics: Conference Series*, volume 1693, page 012135. IOP Publishing.
- Zhang, D., Huang, G., Zhang, Q., Han, J., Han, J., Wang, Y., and Yu, Y. (2020). Exploring task structure for brain tumor segmentation from multi-modality mr images. *IEEE Transactions on Image Processing*, 29:9032–9043.
- Zhao, L., Wu, W., and Corso, J. J. (2013). Semi-automatic brain tumor segmentation by constrained mrfs using structural trajectories. In *International Conference on Medical Image Computing and Computer-Assisted Intervention*, pages 567–575. Springer.
- Zikic, D., Glocker, B., Konukoglu, E., Criminisi, A., Demiralp, C., Shotton, J., Thomas, O. M., Das, T., Jena, R., and Price, S. J. (2012). Decision forests for tissue-specific segmentation of high-grade gliomas in multi-channel mr. In *International Conference on Medical Image Computing and Computer-Assisted Intervention*, pages 369–376. Springer.